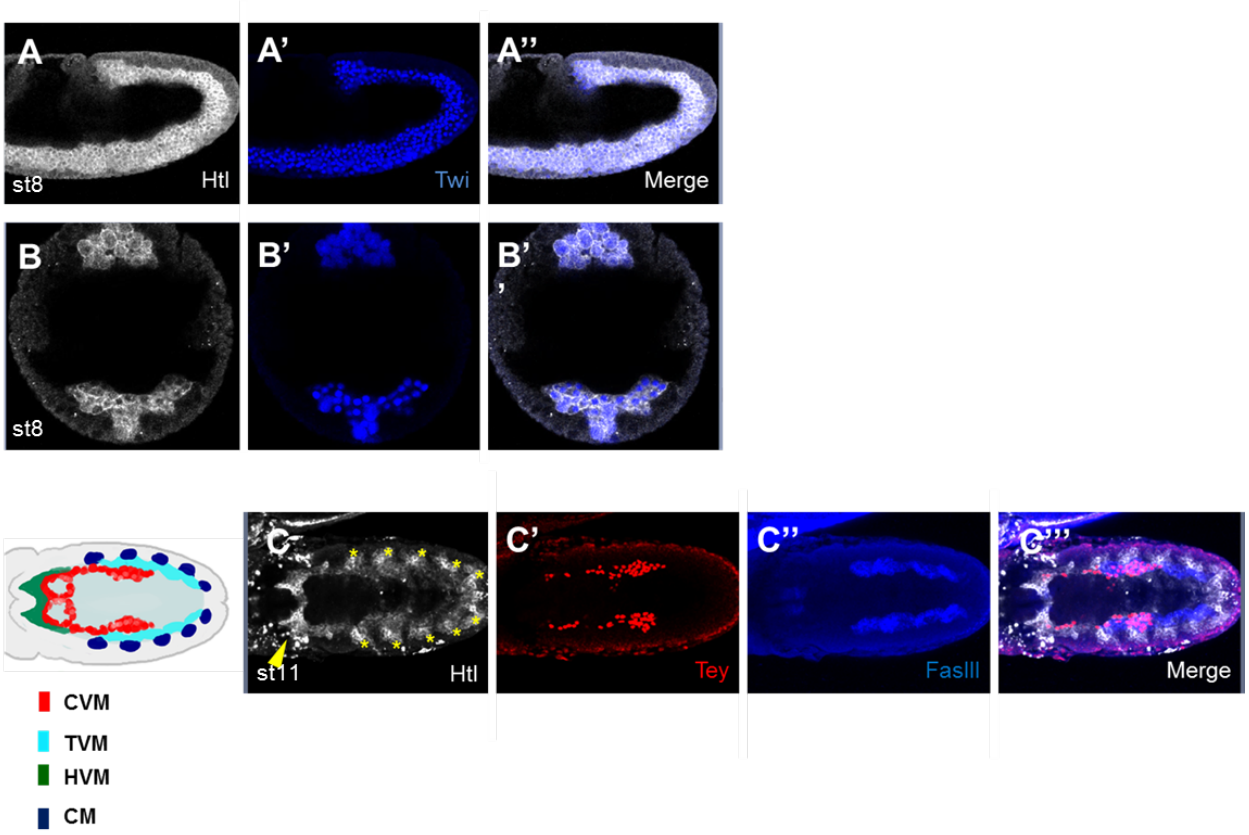

Figure S1. Htl antibody staining pattern in stage 8 and stage 11 embryos. (A-A'', B-B'') Sagittal and transverse confocal cross-sections of stage 8 embryos immunostained against Htl (white) and Twi (blue) demonstrating Htl protein localization throughout the mesoderm. (C-C''') Coronal confocal cross-section of a stage 11 embryo immunostained against Htl (white), Tey (CVM, red), and FasIII (TVM, blue) demonstrating refinement of Htl protein localization to the hindgut visceral mesoderm (HVM, yellow arrowhead), CVM (region overlapping with Tey antibody staining), and cardiogenic mesoderm (CM, yellow asterisks).

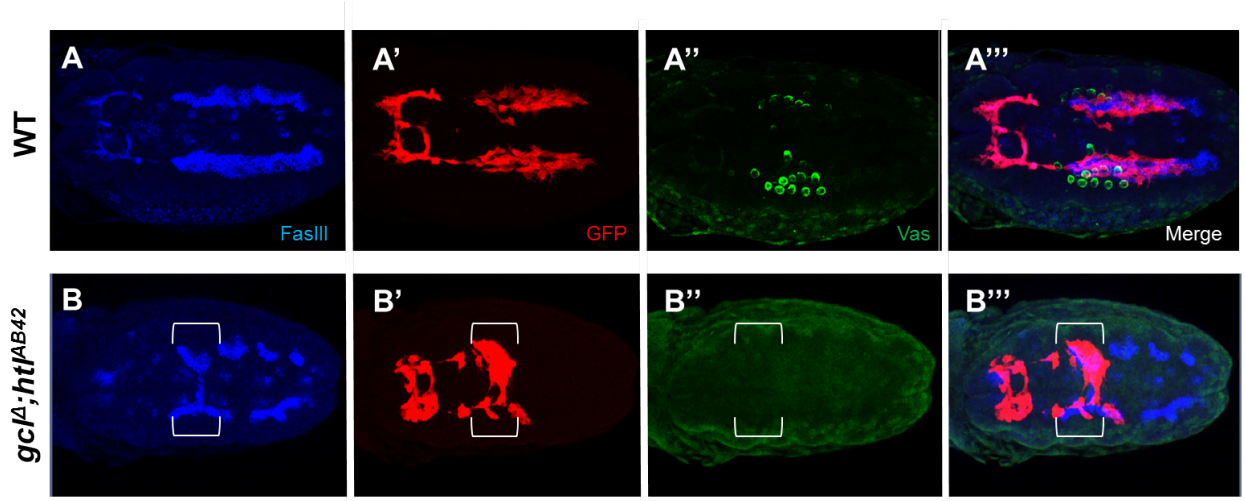

Figure S2. Loss of PGCs does not attenuate CVM and TVM midline crossing and contralateral merging defects. (A-A''', n=6) *yw*/GV2 embryo immunostained against FasIII (TVM), GFP (CVM), and Vasa (PGCs). PGCs co-migrate into two groups along with the CVM. (B-B''', n=4) Immunostained *gclΔ*/*CyO*;*htl*^{AB42} embryo demonstrating persistence of CVM midline crossing and TVM contralateral merging phenotypes in the absence of PGCs.

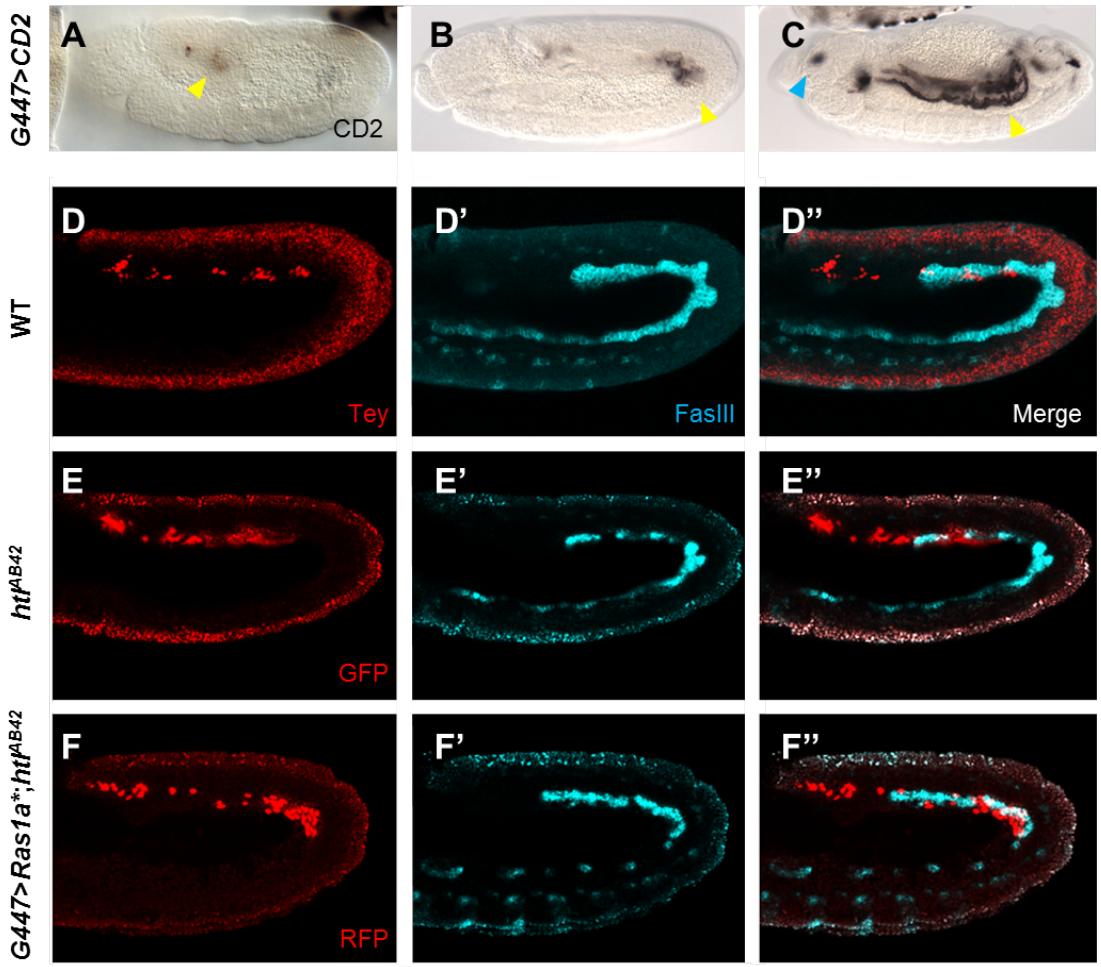

Figure S3. CVM-specific rescue of FGF activity correlates with attenuation of TVM ipsilateral gap defect. (A-C) Colorimetric immunostainings of *G447-GAL4* driving *CD2* expression to demonstrate specificity of driver. Expression is predominantly CVM-specific at these stages (yellow arrowheads), with the exception of a small anterior population of cells (blue arrowhead). (D-F'') Sagittal confocal cross-sections of stage 11 embryos immunostained against FasIII to label the TVM and either Tey (no reporter), GFP (HLH54F-Gap-Venus reporter), or RFP (HLH54F-H2A-mCherry reporter) to label the CVM. In WT embryos, the TVM fuses completely well before the conclusion of stage 11 (D-D'', n=10), while in htl^{AB42} mutants, ipsilateral gaps are

present along the length of the embryo, which the CVM cells traverse (E-E'', n=11). When MAPK signaling is partially restored in the CVM via targeted expression of constitutively-active *Ras85D*, attenuation of the TVM ipsilateral gap phenotype correlates with position of the migrating CVM cohort (F-F'', n=8).

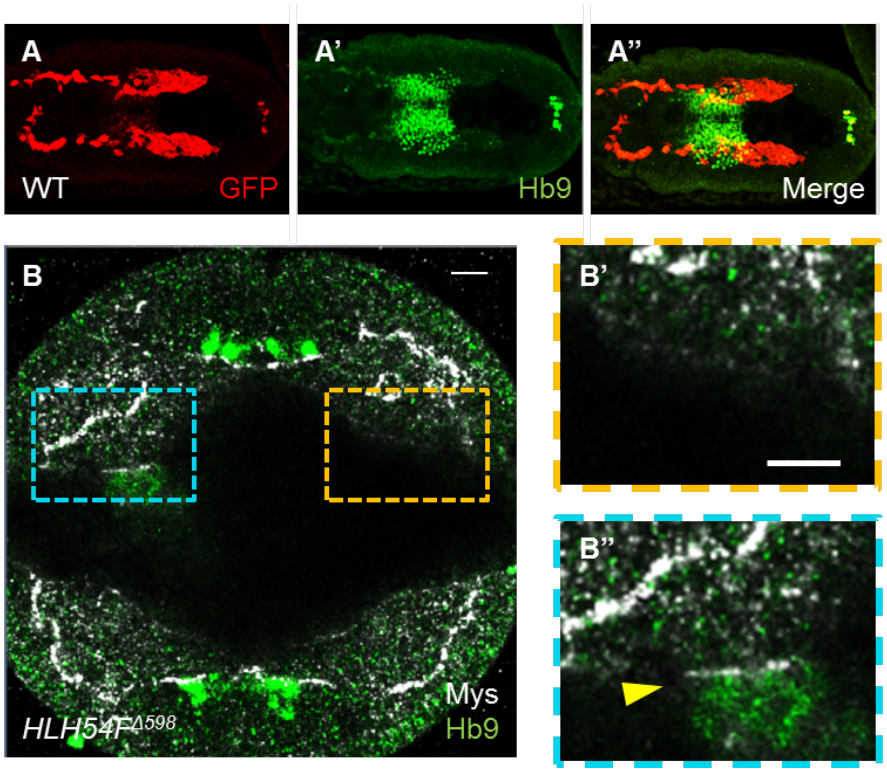

Figure S4. CVM initially migrate along the gut and may interact with TVM in the absence of CVM. Dorsal views of stage 11 WT embryo expressing a GFP CVM reporter immunostained against GFP (CVM) and Hb9 (gut) demonstrating proximity of CVM and gut (A-A''). (B-B'') Transverse view of immunostained *HLH54F* mutant embryo stained against Mys (βPS1) and Hb9 (gut), sliced in such a way that one side of the embryo demonstrates contact of the trunk mesoderm and a lobe of the gut (B'') and the other side does not show contact between the trunk mesoderm and gut (B'). Contact between the gut and mesoderm apparently restores some polarized integrin expression even in the absence of CVM (yellow arrowhead). (Scale bars, 10μm)

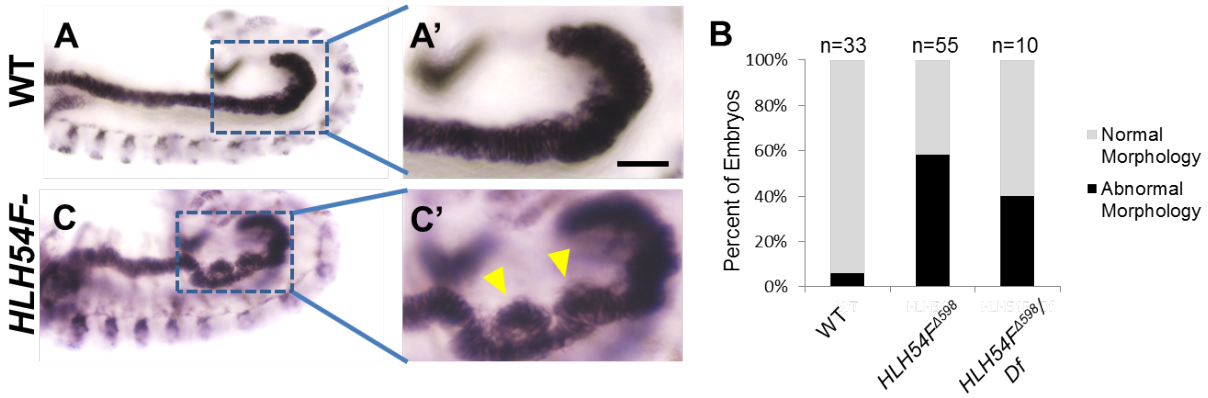

Figure S5. Loss of CVM results in TVM morphology defects. Sagittal sections of late stage 12 embryos immunostained against FasIII to visualize the TVM. In WT embryos, the circular muscle precursors form a continuous, relatively linear structure (A-A', B). In *HLH54F* mutants, the circular muscle precursors often present an aberrant, convoluted morphology (B, C-C', yellow arrowheads) *Df = Df(2R)Exel7150*, a deficiency that removes *HLH54F*. (Scale bars, 20µm)

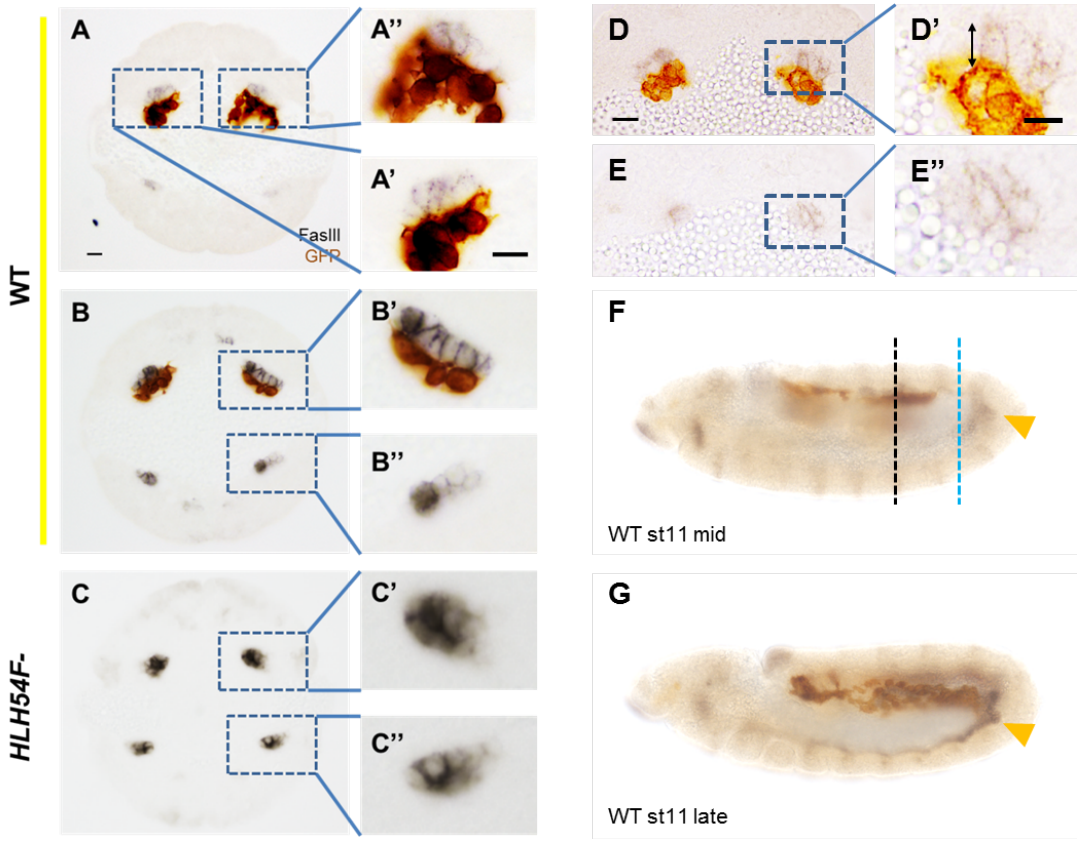

Figure S6. TVM morphological changes correlate with CVM position. (A-C) Transverse sections of stage 11 embryos immunostained against FasIII to visualize the TVM and GFP to visualize the CVM. In WT embryos, the TVM cells that are in contact with the CVM present more elongated shapes (A'-A'', B') compared to the TVM cells ahead of the migrating CVM (B''). This can be observed even in an earlier stage 11 embryo, in which TVM cells attached to CVM also show more elongated shapes compared to TVM not yet reached by the CVM (D-E''; black dotted line vs. blue dotted line in F). FasIII staining is weaker in mid-stage 11 embryos compared to late stage 11 (F, G, orange arrowheads). In *HLH54F* mutants, TVM cell shape appears to be irregular throughout (C', C''). (Scale bars, 10µm)